Hydrogen-rich Syngas Production *via* Catalytic Gasification of Biomass Using Ni/Zr-MOF Catalyst

Shuang Shang, Zhenhua Qin, Kui Lan, Yan Wang, Juanjuan Zhang, Tao Xiong, Weitao He, and Jianfen Li *

A Ni/Zr-MOF catalyst supported on Zr-metal organic framework (Zr-MOF) was prepared by a homogeneous precipitation method and was used in the co-gasification of wet sludge and straw. The Ni/Zr-MOF catalyst was characterized *via* thermogravimetric, X-ray diffraction, scanning electron microscopy, energy dispersive spectrometry, and Brunauer-Emmett-Teller analyses. The experimental results illustrated that the Zr-MOF crystals were an octahedral structure with a specific surface area of 806 m^2/g, and had mesoporous structure. Nickel was uniformly dispersed on the surface of the catalyst, and most of the Ni/Zr-MOF crystals maintained an octahedral morphology. Compared with non-catalyst biomass gasification, the H_2 yield increased from 0.39 mol/kg to 11.87 mol/kg using the Ni/Zr-MOF catalyst at 500 °C. After 10 instances of reuse, the H_2 yield was still as high as 10.11 mol/kg. The Ni/Zr-MOF catalyst exhibited high catalytic activity and stability for biomass gasification at low-temperature.

Keywords: Gasification; Biomass; Zr-MOF; Catalyst; Syngas

*Contact information: School of Chemical and Environmental Engineering, Wuhan Polytechnic University, Wuhan 430023, China; *Corresponding author: lijfen@163.com*

INTRODUCTION

Energy and environment issues are current topics of concern in society. With the rapid development of the economy, fossil fuels, as non-renewable sources of energy, have been unable to meet the growing demand for energy. Long-term development and use of fossil energy will face the problem of fuel depletion, and oil reserves are estimated to be depleted by 2050 (Saxena *et al.* 2009). Biomass is a renewable material that can be converted into solid, liquid, and gaseous fuels through chemical processes (Guan *et al.* 2016). Biomass pyrolysis or gasification is one of the most effective ways to convert biomass into fuel (Ismail and El-Salam 2017). Pyrolysis can make full use of biomass raw materials. The products are gas, tar, and char, and the process does not form toxic and harmful organic compounds (Xu *et al.* 2017). The problem with pyrolysis is its low content of flammable gases in the product gas, such as H_2 and CO. Additionally, a large amount of tar in the gas phase will condense at low temperatures, blocking the downstream pipeline of the process. In addition, tar can cause a lot of energy loss and some environmental problems related to tar (Han and Kim 2008). Catalytic cracking has high cracking tar efficiency and gas reforming ability. Converting tar into useful syngas is a technically feasible and economical gas purification technology (Zhou *et al.* 2017).

Ni-based catalysts have attracted much attention for tar cracking and gas purification due to their high catalytic activity and relatively low cost. Some studies also show that Ni-based catalysts can reverse ammonia reaction; thus, it is possible to reduce NO_x emission during biomass gasification and tar reforming (Shen and Yoshikawa 2013).

The traditional Ni-based catalyst supports are mainly metal oxide (γ-Al_2O_3, CeO_2, and MgO) and natural materials (palygorskite, dolomite, and olivine). The accommodation of Ni in the support could improve Ni dispersion, suppress the aggregation of metal particles, and control the particle size efficiently (Zhang *et al.* 2018).

In recent years, char has also been used as the support for Ni-based catalysts due to its pore structure and large specific surface area. Hu *et al.* (2018) prepared Ni/char catalysts using pine sawdust char as the catalyst support. The results showed that the char-supported nickel catalysts had high catalytic activity in biomass gasification and tar removal. Shen *et al.* (2014) prepared a Ni-Fe/RHC catalyst using rice husk char (RHC) as the support. It was found that rice husk char can be prepared as a highly porous carbonaceous material, like activated char. The support with a larger specific surface area can promote the dispersion of metal elements on the surface of the catalyst; at the same time, a larger pore size is beneficial to the diffusion of reactants and products in the channel of the catalyst. Xie *et al.* (2018) used carbon nanofiber (CNF) as the catalyst support to prepare an Fe-Ni/CNF catalyst and applied it to the catalytic conversion of tar from biomass gasification. The experimental results indicated that the Brunauer-Emmett-Teller (BET) surface area and average pore diameter of Fe-Ni/CNF was 283 m^2/g and 3.73 nm, respectively. The syngas yield increased from 0.3 to 0.7 L/g using an Fe-Ni/CNF catalyst. For the same metal loading, a support with a larger specific surface area can provide more active sites, and the catalytic activity of the resulting catalyst is higher. Therefore, to improve the catalytic activity of catalysts, researchers have prepared many synthetic materials with high specific areas, such as SBA-15, ZSM-5, MCM-41, *etc*. Zhang *et al.* (2019) prepared Ni/Al_2O_3 and Ni/SBA-15 catalysts with 20% nickel loading using Al_2O_3 and SBA-15 as a support to compare the effect of support on catalytic activity. The results showed that the BET surface area of Ni/SBA-15 (333.1 m^2/g) was higher than that of Ni/Al_2O_3 (139.9 m^2/g), and the Ni/SBA-15 catalyst showed superior activity to that of the Ni/Al_2O_3 catalyst. Wu *et al.* (2011) prepared Ni/MCM-41 catalysts using MCM-41 as support for sawdust gasification to produce hydrogen. The results showed that Ni/MCM-41 catalysts had higher specific surface areas (> 737 m^2/g), and the NiO particles had good dispersion on the surface of the support.

The Zr-metal organic framework (Zr-MOF) material has an octahedral structure, and its specific surface area could reach 1367 m^2/g (Ren *et al.* 2014). The uniform structure and larger specific surface area of Zr-MOF material enable the metal to be evenly dispersed on the surface of the support, and the rich pore structure can make the tar fully contact with the catalyst. In addition, presently, Zr-MOF material is mainly used for hydrogen storage, but it has not been used in the study of biomass catalytic gasification for hydrogen production. Therefore, in this work, an Ni/Zr-MOF catalyst was prepared using synthesized Zr-MOF materials as support and applied to the co-gasification of wet sludge and wheat straw.

The Ni/Zr-MOF catalyst was characterized by thermogravimetric (TG), X-ray diffraction (XRD), scanning electron microscopy (SEM), energy dispersive spectrometry (EDS), and BET analyses to explore the mechanism of the catalyst. A series of experiments were performed to explore the effects of the catalyst on the composition and yield of gases, Ni loading, cycle stability of catalyst and catalyst regeneration. Meanwhile, a non-catalyst was also studied as the baseline for comparison.

EXPERIMENTAL

Materials

The wet sludge used in this study was collected from a domestic sewage treatment plant in Wuhan, Hubei Province, China. The sludge was dried at 105 °C for 24 h in an oven to ensure that their mass was constant. The wet sludge with a moisture content of 80% was obtained by uniformly mixing the dry sludge with a certain amount of water. The wheat straw selected from Wuhan, China was pulverized to the size of 0.3 mm to 4.0 mm with a small crusher to eliminate the influence of the particle size on the experimental results. The biomass sample obtained by mixing wheat straw and wet sludge with a moisture content of 80% was used as the raw material for hydrogen-rich syngas production. The proximate and ultimate analyses of dry sludge and wheat straw are listed in Table 1 and presented on an air-dried basis.

Table 1. Proximate and Ultimate Analysis of Dry Sludge and Wheat Straw

Sample	Proximate Analysis (wt%)				Ultimate Analysis (wt%)				
	M^{ad}	A^{ad}	V^{ad}	$C_F{}^{ad}$	C	H	N	S	O[c]
Sludge	4.15	50.69	35.33	9.83	25.20	5.62	3.82	0.15	14.52
Wheat Straw	10.88	6.91	67.11	15.10	31.04	4.22	0.40	0.06	57.37

M (Moisture); A (Ash); V (Volatile); C_F (Fixed carbon); [ad] Air-dried; [c] Calculated by difference (O% = 100%－Ash%－C%－H%－N%－S%)

Methods

Catalysts preparation

The highly ordered mesoporous Zr-MOF was synthesized by the solvothermal method reported previously (Ren *et al.* 2014). Approximately 2.34 g of $ZrCl_4$ and 1.66 g of terephthalic acid were ultrasonically dissolved in 100 mL of N,N-dimethylformamide (DMF) solvent. Approximately 38 mL of formic acid was added as the modulator. The solution was transferred to a Teflon-lined pressure vessel before being heated up to 120 °C and maintained at that temperature for 24 h under static conditions. After cooling, the white product was collected by centrifugation, washed twice with 200 mL DMF and 200 mL ethanol, and then dried for 12 h in an oven at 60 °C.

The Ni/Zr-MOF catalyst was prepared by the homogeneous precipitation method using $Ni(NO_3)_2{\cdot}6H_2O$ as the nickel precursor. The nickel loading was 20 wt%. A certain proportion of $Ni(NO_3)_2{\cdot}6H_2O$ and Zr-MOF material was added in a 500-mL flask. Then, 4 g of potassium hydroxide as precipitant and 400 mL of distilled water were added. The blend was stirred at 115 °C for 3 h and precipitated for 1 h. After filtering and drying overnight at 105 °C, the Ni/Zr-MOF catalyst was devolatilized in a flowing nitrogen atmosphere from ambient temperature to 500 °C at 10 °C/min, and then held at 500 °C for 2 h before being stored and used further.

Apparatus and procedure for biomass gasification

The experiments were performed using a fixed bed reactor facility, as shown in Fig. 1. The biomass sample (1 g of wet sludge with a moisture content of 80% and 1 g of wheat straw) and quartz wool (Daiermeng Science and Technology, Wuxi, China) containing 1 g of Ni/Zr-MOF catalyst was placed in a porcelain boat. Before the experiment, high-purity nitrogen gas was introduced into the quartz tube for 30 min to exhaust the air in the quartz tube. The experiments were performed at 500 °C. The holding time was set to 10 min. Once

the desired temperature was reached, the heating furnace was pushed to the position where the sample was located, and it was instantly gasified at the specified temperature. The non-condensable gases were collected with a gas collecting bag and the volume of produced gas was measured by a gas flow meter. The composition and content of the gas were measured by a gas analyzer.

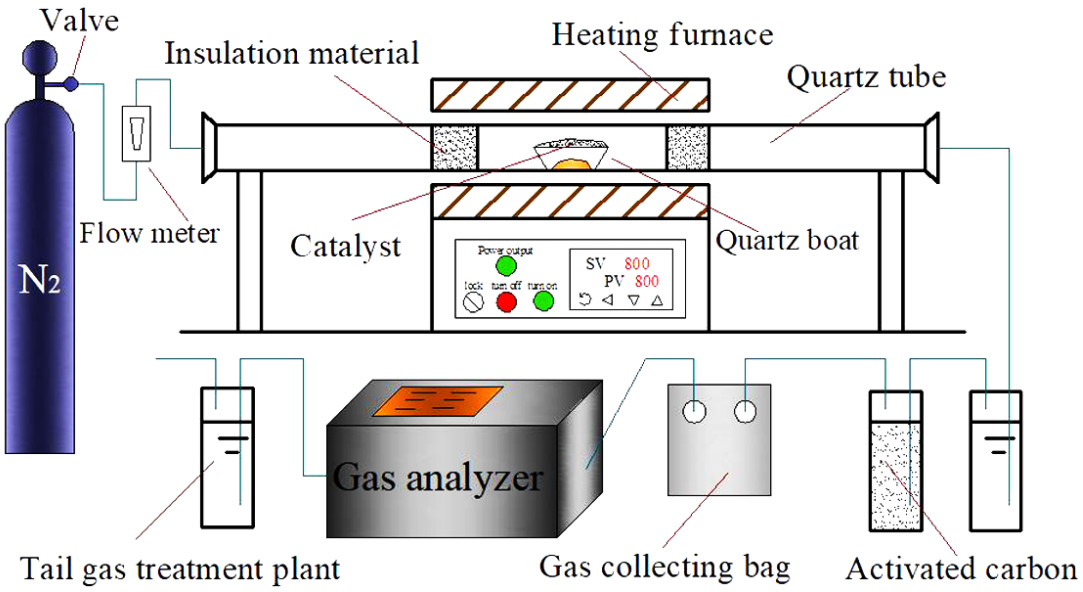

Fig. 1. Schematic diagram of the experimental system

Methods

Analysis

The ultimate analysis of the samples was conducted with a CHNS/O analyzer (FLASH2000; Thermo Fisher Scientific, Waltham, MA, USA). This analysis simultaneously gave the mass percentages of carbon, hydrogen, nitrogen, and sulfur in the samples, and the mass percent of oxygen was determined by the difference. The proximate analysis method of coal, according to GB/T 212 (2008), was used to obtain a proximate analysis of the sludge and wheat straw (*i.e.*, moisture, volatile matter, fixed carbon, and ash content of the material). The material structure of the Ni/Zr-MOF catalyst was analyzed using an X-ray diffractometer (XRD-7000; Shimadzu Corp., Kyoto, Japan). The thermal stability of the support and catalyst were evaluated using a thermogravimetric analyzer (SDT Q600; TA Instruments, New Castle, DE, USA). Scanning electron microscopy (S9000; Tescan, Ltd., Brno, Czech) equipped with EDS was used to observe the surface morphology of the support and catalyst. The surface area and pore properties of the support and catalyst were determined by a surface area analyzer (ASAP 2020 HD88; Micromeritics Instrument Corp., Norcross, GA, USA). The gas composition analysis was conducted with an infrared gas analyzer (Gasboard-3100P; Hubei Cubic-Ruiyi Instrument Co., Wuhan, China). The lower heating value (LHV) of the product gas is defined by Lv *et al.* (2004) as follows,

$$\mathrm{LHV\ (kJ/Nm^3)} = (27.5 \times \mathrm{H_2} + 30 \times \mathrm{CO} + 85.4 \times \mathrm{CH_4} + 151.3 \times \mathrm{C_nH_m}) \times 4.2 \quad (1)$$

where H_2, CO, CH_4, and C_nH_m are the gas concentrations (vol%) of the product gas.

RESULTS AND DISCUSSION

Characterization of Catalysts

TG analysis

Figure 2 shows the thermogravimetric analysis of the Zr-MOF support and Ni/Zr-MOF catalyst under the N_2 atmosphere. As shown by the dotted line in Fig. 2, with the increase of temperature, the TG profile of Ni/Zr-MOF catalyst was an almost horizontal straight line, which showed that the quality of the catalyst was almost unchanged. Consequently, the Ni/Zr-MOF catalyst had a high thermal stability. As shown by the solid line in Fig. 2, the Zr-MOF support presented mainly two stages in weight loss. The TG profile of Zr-MOF support obtained in this experiment was consistent with the results reported by Ren *et al.* (2014). A continuous mass loss of Zr-MOF support before 350 °C likely corresponded to the removal of all organic material, including the evaporation of guest molecules from the pores such as the solvent DMF. Between temperatures of 350 °C and 500 °C the mass loss was almost linear, which indicated that the Zr-MOF support had high thermal stability under 500 °C. The Zr-MOF support maintained their structure up to 500 °C and after that a sudden weight loss was observed, which was attributed to decomposition of the Zr-MOF to ZrO_2.

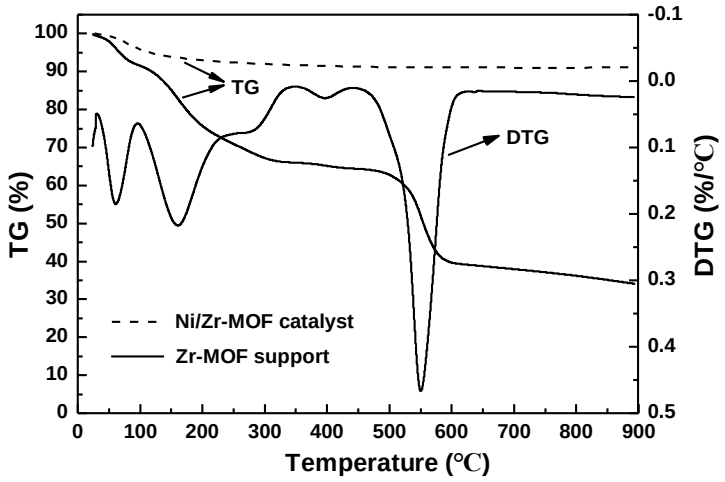

Fig. 2. TG analysis of Zr-MOF support and Ni/Zr-MOF catalyst under the N_2 atmosphere

XRD analysis

Figure 3 shows the XRD patterns of three catalysts and Ni/Zr-MOF catalysts with different Ni loading. As shown in Fig. 3(a), in the Ni/Zr-MOF catalyst, the peaks at 2θ = 37.3°, 43.3°, 62.8°, 75.4°, and 79.5° were observed and identified as NiO (PDF#89-5881). According to the Scherrer formula, the average size of the NiO grains in the Ni/Zr-MOF catalyst was approximately 10 nm, which indicated that NiO had good dispersion on the Zr-MOF support. After catalytic cracking, the active components of Ni/Zr-MOF catalyst had changed. The characteristic diffraction peaks of Ni (111), Ni (200), and Ni (220) at 2θ = 44.4°, 51.6°, and 76.1° (PDF#01-1258), respectively, were observed in the used Ni/Zr-MOF catalyst. The average size of the Ni grains was approximately 12 nm, which indicated that the metal nickel might agglomerate after 10 instances of reuse. The conversion of NiO to Ni was attributed to carbothermal reduction and hydrogenation reduction. Hu *et al.* (2018) showed that NiO was transformed into Ni, which contributed to the enhancement

of tar conversion. In addition, the strong peaks at 2θ = 30.1°, 34.9°, 50.2°, and 59.7° were observed and identified as ZrO_2 (PDF#89-9069), which indicated that the Zr-metal organic framework was decomposed into ZrO_2, and the metal organic framework might collapse. The characteristic diffraction peaks of NiO at 2θ = 37.2°, 43.9°, 62.9°, 75.4°, and 79.5° (PDF#89-7131), respectively, were observed in the regenerated catalyst. What's more, the characteristic peak intensity of NiO in the regenerated catalyst was higher than that of the Ni/Zr-MOF catalyst. As shown in Fig. 3(b), the NiO characteristic peaks became stronger and narrower with the increase of Ni loading.

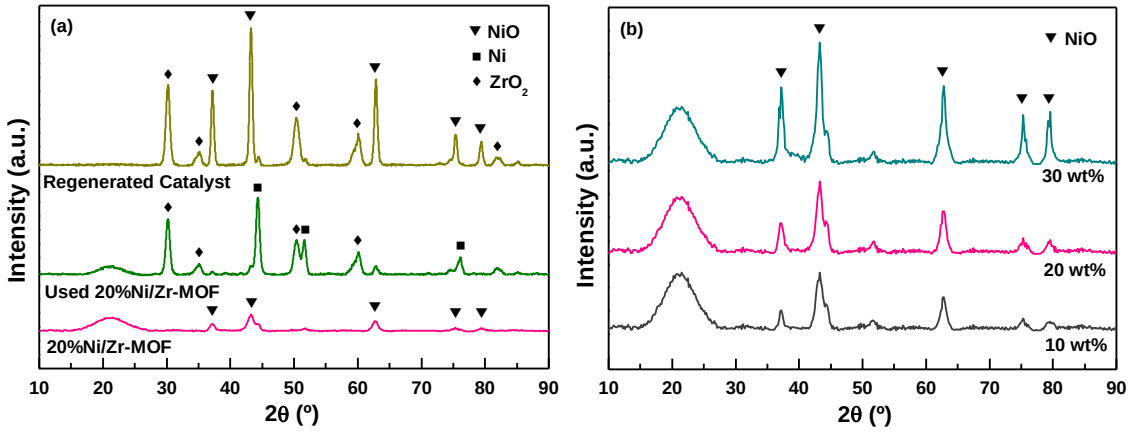

Fig. 3. XRD patterns of (a) three catalysts, and (b) Ni/Zr-MOF catalysts with different Ni loading

SEM-EDS analysis

Figure 4 shows the SEM images of the Zr-MOF support, Ni/Zr-MOF catalyst, and used Ni/Zr-MOF catalyst. Figure 4(a) shows that all of the Zr-MOF crystals took an octahedral shape with particle sizes of approximately 100 nm. The analysis of Ni/Zr-MOF catalyst *via* SEM-EDS indicated that the octahedral morphologies of the Zr-MOF crystals were maintained, and nickel was uniformly dispersed on the surface of the Zr-MOF support, which provided more active sites for the Ni/Zr-MOF catalyst. Moreover, the pore structure of the Ni/Zr-MOF catalyst was still clear, which is conducive to the diffusion of tar in the catalyst. This is noticeable in the SEM image and was confirmed by the EDS analysis (Fig. 4(b)). According to EDS analysis, the metal nickel had been successfully loaded on the Zr-MOF support. However, it can be observed from Fig. 4(c) that most of the octahedron structure of the Ni/Zr-MOF catalyst collapsed after reuse. Additionally, only the Zr-MOF crystal with the larger particle size retained the octahedron structure, and the agglomeration of nickel resulted in the increase of particle size.

BET analysis

The N_2 adsorption and desorption isotherms of the Zr-MOF support, Ni/Zr-MOF catalyst, and used Ni/Zr-MOF catalyst, are presented in Fig. 5. The pore sizes of the three samples were mainly distributed between 0 nm to 50 nm. Additionally, all the isotherms were of the type 4 pattern according to the IUPAC classification, which corresponded to the mesoporous structure of the three samples. The mesoporous structure of the Ni/Zr-MOF catalyst had adsorption capacity for tar, which could promote the contact between tar and active components to produce more hydrogen-rich syngas from cracking tar.

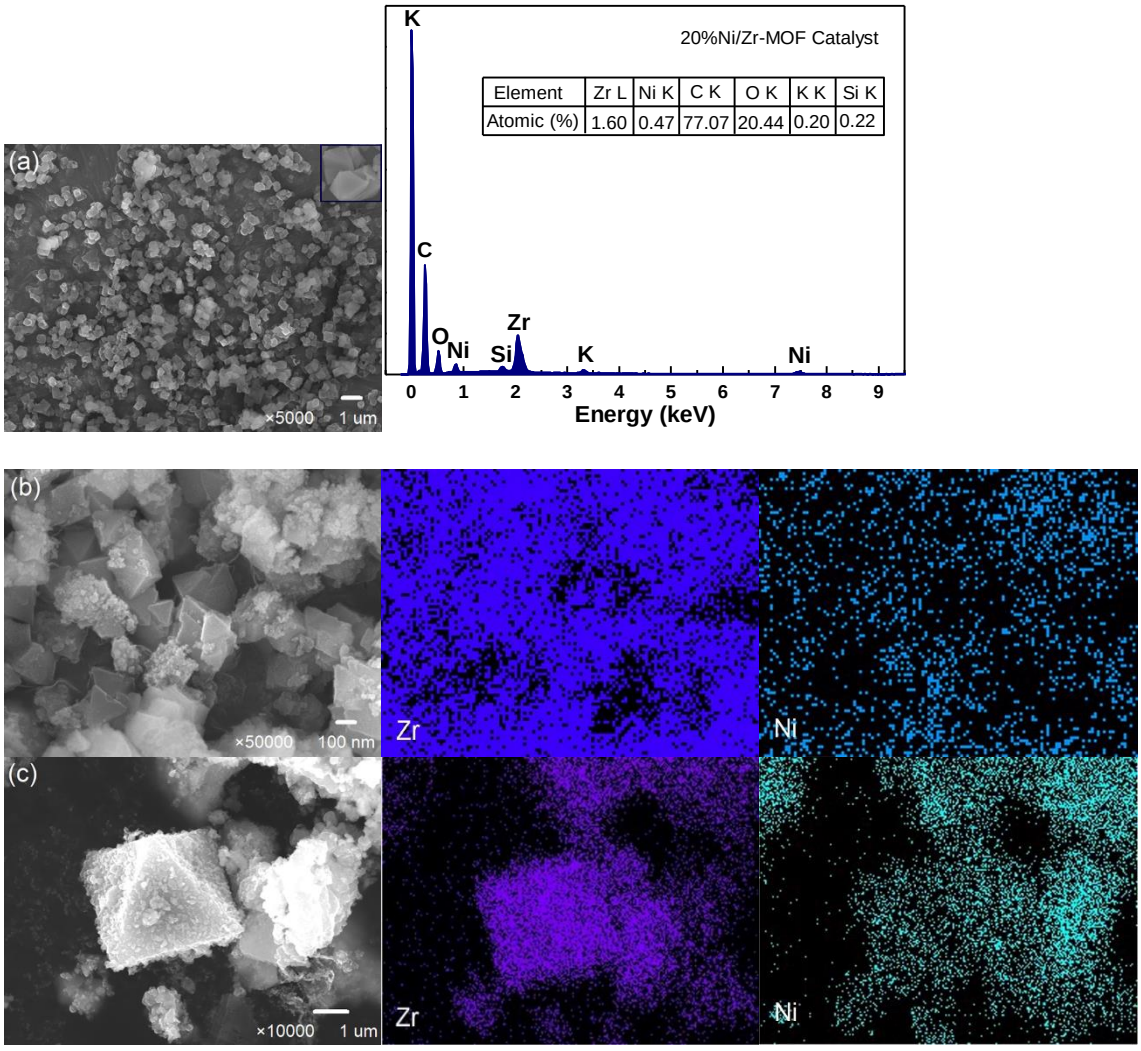

Fig. 4. SEM image of (a) Zr-MOF support, SEM-EDS images of (b) Ni/Zr-MOF catalyst, and (c) used Ni/Zr-MOF catalyst

The textural parameters of Zr-MOF support, Ni/Zr-MOF catalyst, and used Ni/Zr-MOF catalyst, including BET surface area, total pore volume, and average pore diameter, are listed in Table 3. It was found that the BET surface area of Zr-MOF support was 806 m^2/g, the pore volume was 0.47 cm^3/g, and the pore diameter was 20.14 nm. A large number of studies have shown that supports with larger BET surface areas can promote the dispersion of metal elements on the surface of a catalyst, and a larger pore diameter is beneficial to the diffusion of reactants and products in the channel of catalyst, so as to improve the catalytic activity of the catalyst (Shen *et al.* 2011). Furthermore, it was found that the BET surface area and pore volume of the Ni/Zr-MOF catalyst decreased after reuse. Carbon deposition of the Ni/Zr-MOF catalyst blocked some micropores, which resulted in a decrease in the BET surface area. Compared with the fresh Ni/Zr-MOF catalyst, the used Ni/Zr-MOF catalyst had a larger pore diameter due to the destruction of the Zr-MOF support structure after reuse.

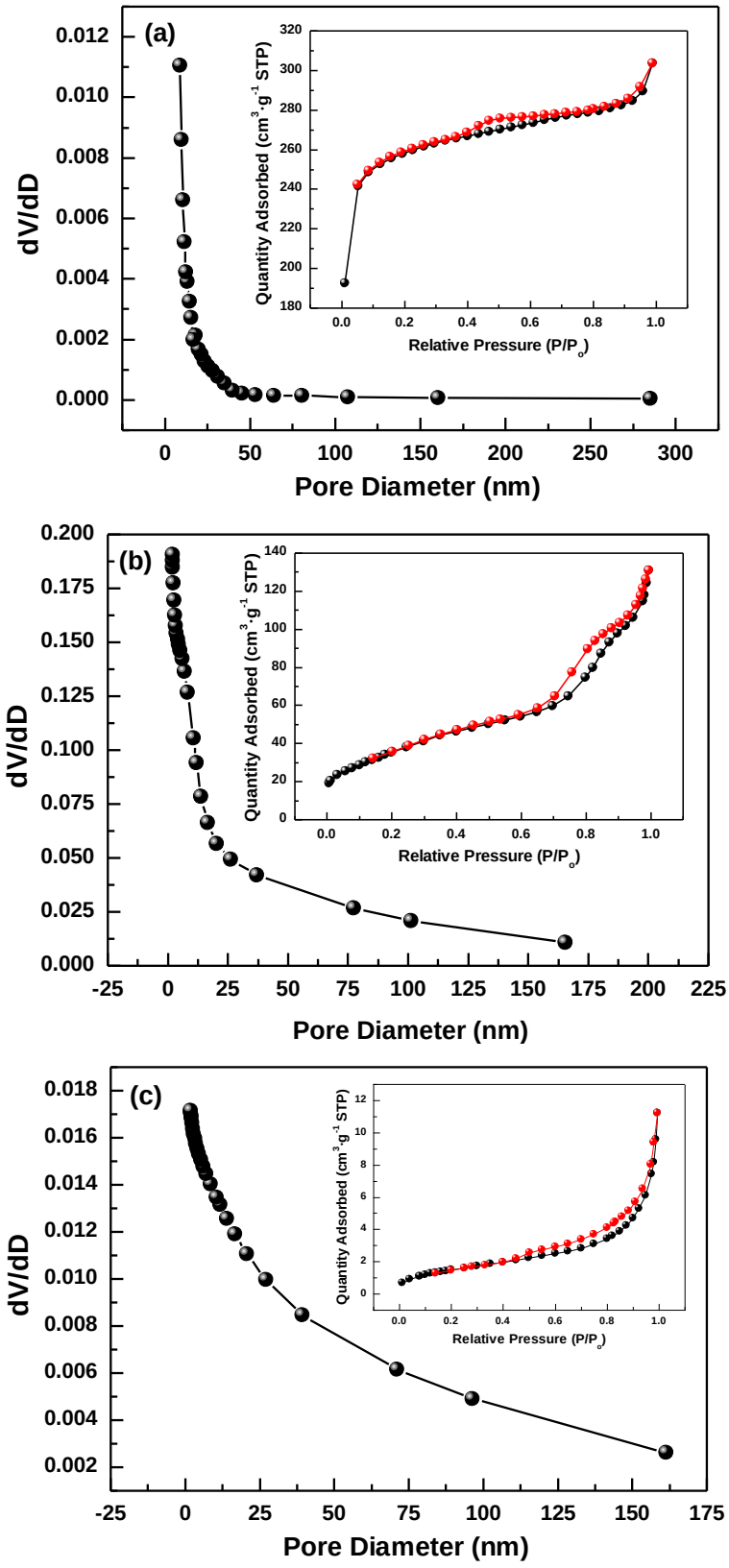

Fig. 5. N_2 adsorption-desorption isotherm plots and pore distribution of Zr-MOF support (a), Ni/Zr-MOF catalyst (b), and used Ni/Zr-MOF catalyst (c)

Table 2. Textural Parameters of Zr-MOF Support, Ni/Zr-MOF Catalyst, and Used Ni/Zr-MOF Catalyst

Sample	BET Surface Area (m^2/g)	Total Pore Volume (cm^3/g)	Average Pore Diameter (nm)
Zr-MOF	805.9	0.47	20.14
Ni/Zr-MOF Catalyst	132.7	0.19	7.39
Used Ni/Zr-MOF Catalyst	5.64	0.02	11.96

Application and Analysis of Ni/Zr-MOF Catalyst in Biomass Gasification

The important reactions that took place during catalytic gasification of wet sludge and wheat straw were summarized as follows (Hu *et al.* 2015; Yang *et al.* 2018):

Drying process: Wet sample → steam + dry sample (2)

Pyrolysis: Dry sample → gas + tar + char (3)

Secondary cracking: Tar → $H_2 + CO + CO_2 + CH_4 + H_2O + C_nH_m$ (4)

Steam gasification reaction: $C_nH_m + nH_2O + Q \rightarrow nCO + [n + (m/2)]H_2$ (5)

Methane reforming reaction: $CH_4 + H_2O \rightarrow CO + 3H_2 + 206\ kJ/mol$ (6)

Water gas shift reaction: $CO + H_2O \rightarrow CO_2 + H_2 - 41\ kJ/mol$ (7)

Char steam gasification reaction: $C + H_2O \rightarrow CO + H_2 + 131\ kJ/mol$ (8)

Boudouard reaction: $C + CO_2 \rightarrow 2CO + 172\ kJ/mol$ (9)

Figure 6 shows the processes of biomass catalytic gasification. First, the drying process of the wet sample took place at a high temperature, which formed *in-situ* steam around the sample (Eq. 2). Meanwhile, the dry sample was rapidly pyrolyzed to gas, tar, and char (Eq. 3), followed by secondary cracking of the tar to form gas and small molecule organic matter (Eq. 4), steam gasification reaction, methane reforming reaction, water gas shift reaction, char steam gasification reaction, and the Boudouard reaction (Eqs. 5 through 9).

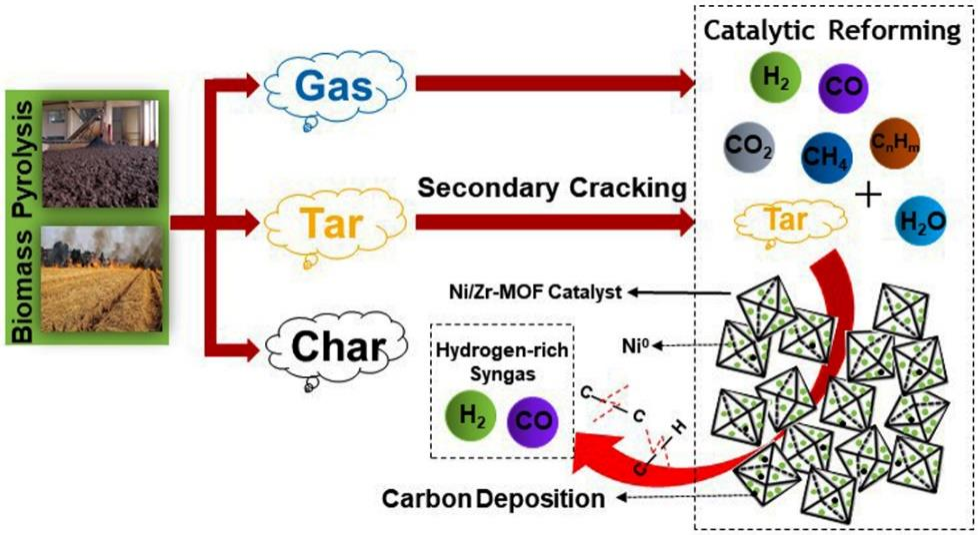

Fig. 6. Mechanism of catalytic gasification of biomass using Ni/Zr-MOF catalyst

The primary gas was produced from the thermal scission of chemical bonds in the individual constituents of biomass, when catalytic reforming reactions cleaved the C—C and C—H bonds of the carbohydrate backbone to produce CO and H_2 (Kunkes *et al.* 2008). Due to the presence of *in-situ* steam, the char steam gasification reaction not only could refresh the active surface area of the catalyst by reducing the carbon deposit of the catalyst, but it also increased the CO and H_2 content in the gas.

Influence of catalyst on gas composition

The Ni/Zr-MOF catalyst was used for tar cracking and improving gas quality in the catalytic *in-situ* steam gasification of wet sludge and straw, compared with the case without catalyst. The influence of the Ni/Zr-MOF catalyst on gas composition and characterization under 500 °C are shown in Fig. 7 and Table 3. The main components in the gas were H_2, CO, CH_4, and CO_2, which accounted for more than 98% of the gas, in addition to a small amount of C_nH_m. From the view of overall production, with the addition of the Ni/Zr-MOF catalyst, the dry gas yield showed a noticeable growth trend, from 0.45 to 0.56 $N \cdot m^3/kg$. Additionally, CO was the leading component in hydrogen-rich syngas without the addition of catalyst, accounting for 55.07 vol%. With the Ni/Zr-MOF catalyst, the content of H_2 remarkably increased from 1.94 vol% to 47.49 vol%, and the H_2 yield increased from 0.39 mol/kg to 11.87 mol/kg, while the CO content decreased to 13.15 vol%. The LHV of gas decreased from 15.51 $MJ/N \cdot m^3$ to 12.01 $MJ/N \cdot m^3$, because the calorific values of CH_4 and C_nH_m were higher than that of H_2 or CO. Consequently, the hydrogen-rich syngas yield was dramatically increased under the Ni/Zr-MOF catalyst due to various effects.

First of all, according to the SEM-EDS and BET analyses, the Zr-MOF support had an octahedral structure with a larger specific surface area of 806 m^2/g, which allowed the metal nickel to be uniformly dispersed on the surface of the support, thereby improving the dispersion of metal, increasing the active sites of the catalyst, and improving the activity of the catalyst. Chan and Tanksale (2014) showed that the support material played an important role in defining the activity and service life of the catalyst, and catalysts with high surface area supports generally exhibited higher catalytic activity. Zhao *et al.* (2009) prepared Ni/Al_2O_3 and Ni/MCM-41 catalysts, supported on Al_2O_3 and MCM-41, respectively, which were tested for their performance on the pyrolytic decomposition of cellulose. It was found that the specific surface areas of Al_2O_3 and MCM-41 were 155 m^2/g and 979 m^2/g, respectively. MCM-41 had a highly ordered hexagonal porous structure. The NiO particles were uniformly dispersed on the surface of the MCM-41 support. Furthermore, the shape of the NiO particles was regular, and the pore structure of MCM-41 was the same as that of MCM-41. Compared with the Ni/Al_2O_3 catalyst, the Ni/MCM-41 catalyst could remarkably improve the yield of H_2 and total gaseous products and had a higher catalytic activity for the cracking and reforming of tar and light organic compounds.

Secondly, according to the BET analysis, the pore volume and average pore diameter of the Ni/Zr-MOF catalyst were 0.19 cm^3/g and 7.39 nm, respectively. Therefore, the Ni/Zr-MOF catalyst had a mesoporous structure and good adsorption performance for tar, which promoted the catalytic cracking of tar to produce more hydrogen. In addition, the larger pore diameter was beneficial to the diffusion of reactants and products in the channel of the catalyst. Grams *et al.* (2016) prepared Ni/SBA-15, Ni/SBA-16, Ni/KIT-6, and Ni/MCM-41 catalysts with different mesoporous silica materials as supports, which were used in the thermo-chemical conversion of cellulose to produce hydrogen-rich syngas. The results showed that Ni/SBA-15 and Ni/KIT-6 catalysts had larger pore volumes and pore diameters. The larger pore volumes and pore diameters facilitated

penetration of the catalyst structure by heavier reaction intermediates and full contact with the active site of the catalyst, which allowed for more efficient hydrogen formation. As shown in Table 3, the H_2 yield was remarkably increased from 0.39 mol/kg to 11.87 mol/kg using the Ni/Zr-MOF catalyst. In conclusion, the newly developed Ni/Zr-MOF catalyst had high catalytic performance in the production of hydrogen-rich syngas.

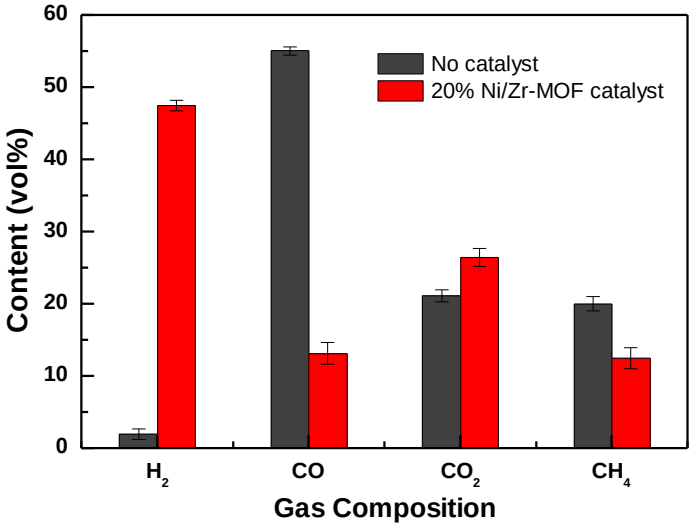

Fig. 7. Influence of catalyst on gas composition

Table 3. Influence of Catalyst on Gas Composition and Gas Characterization

Catalyst	No Catalyst	20%Ni/Zr-MOF Catalyst
Gasification Temperature (°C)	500	500
Catalytic Temperature (°C)	500	500
H_2 Content (vol%)	1.94	47.49
CO Content (vol%)	55.07	13.15
CH_4 Content (vol%)	20.03	12.50
CO_2 Content (vol%)	21.12	26.46
C_nH_m Content (vol%)	1.83	0.40
Dry Gas Yield (N m^3/kg)	0.45	0.56
H_2 Yield (mol/kg)	0.39	11.87
LHV (MJ/N m^3)	15.51	12.01

Influence of Ni loading on syngas conetnt

The influence of Ni loading on syngas content was studied with the Ni/Zr-MOF catalyst under 500 °C. As shown in Fig. 8, when the nickel loading was 0%, the content of H_2 and CO was similar to the case without catalyst, which showed that the Zr-MOF support itself had no catalytic activity. With the increased loading of Ni from 5% to 20%, the H_2 content remarkably increased from 30.57% to 47.49%, which indicated that Ni played a vital role in the promotion of H_2 generation. However, when the Ni loading was further increased from 20% to 30%, the H_2 content showed a slight decrease, from 47.49% to 41.67%. At the same time, it can be found that with the increase of Ni loading, the CO content presented a gradually decreasing trend.

With the increase of Ni loading, the number of active sites in Ni/Zr-MOF catalyst gradually increased, so the catalytic efficiency of the catalyst gradually increased. However, when the Ni loading was too high, a large amount of Ni entered into the pores

of Zr-MOF support, thus blocking the pore structure of catalyst. What's more, Quan *et al.* (2017) showed that high loading of NiO could decrease the dispersion of metal and also increase the aggregation of active sites. Consequently, the active sites which can contact with tar macromolecules will be reduced, thus resulting in the decrease of catalytic activity in Ni/Zr-MOF catalyst. It can be observed from Fig. 3(b) that the NiO characteristic peaks became stronger and narrower with the increase of Ni loading, indicating that the crystal size of NiO particles increased. According to the Scherrer formula, the average size of NiO grains in the Ni/Zr-MOF catalyst was 9 nm, 10 nm, and 12 nm, respectively. Therefore, 20 wt% was the optimal Ni loading for Ni/Zr-MOF catalyst.

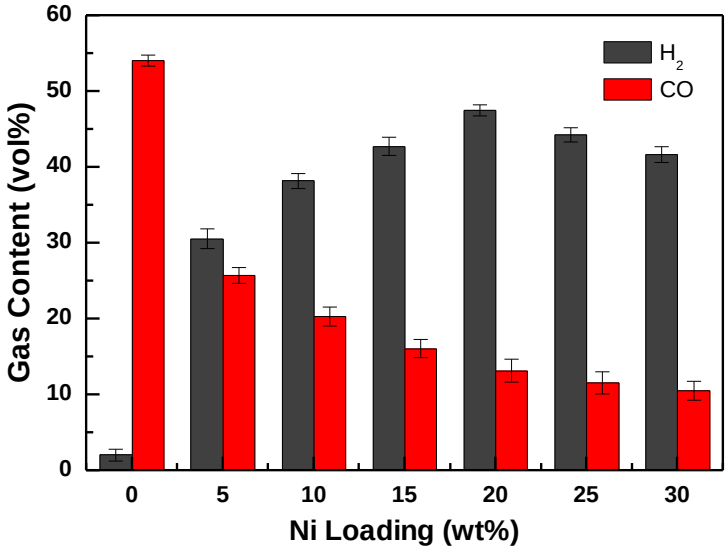

Fig. 8. Influence of Ni loading on syngas content

Catalyst cyclability

The superior catalytic performance of Ni/Zr-MOF has been shown from the above catalyst characterization and experimental results. These results showed that it would be meaningful to further explore its cycling stability. The testing results of the 10-cycling that used Ni/Zr-MOF catalyst are shown in Fig. 9. With the increase of cycle test times, the catalytic performance of the Ni/Zr-MOF catalyst decreased gradually, and the H_2 content decreased from 48.22 vol% to 42.74 vol%. The H_2 yields were, respectively, 12.05 mol/kg and 10.11 mol/kg after the Ni/Zr-MOF catalyst was used one and ten times, and the corresponding H_2 yield was decreased 16.1%.

The 10-cycling that used Ni/Zr-MOF catalyst was characterized by XRD, SEM-EDS, and BET. By comparing the fresh catalyst shown in Fig. 4(b) with the recycle used shown in Fig. 4(c), most of the octahedral morphology of the Ni/Zr-MOF catalyst had collapsed, and the metal nickel had agglomerated. The XRD patterns showed that the active component of the Ni/Zr-MOF catalyst was transformed from NiO to Ni after recycling, which might have consumed a small amount of hydrogen. In addition, the nickel particle size increased from 10 nm to 12 nm, which also confirmed the agglomeration of nickel. This would reduce the active sites of the Ni/Zr-MOF catalyst, thereby reducing the catalytic activity of the catalyst. According to the BET analysis, the pore volume of Ni/Zr-MOF catalyst decreased from 0.19 cm^3/g to 0.02 cm^3/g due to the carbon deposition blocking the pore channel of the catalyst, which was not conducive to the diffusion of tar in the catalyst.

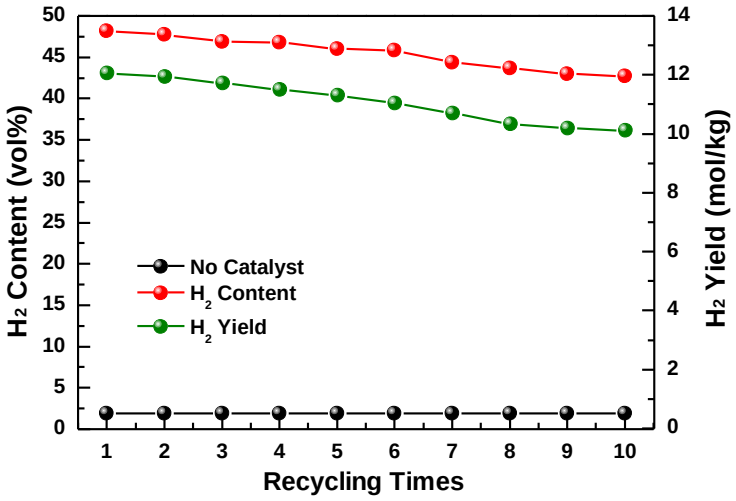

Fig. 9. The H_2 content and H_2 yield of cycling test with 20%Ni/Zr-MOF catalyst under 500 °C

Regeneration of the used catalyst

The catalyst will be deactivated after repeated use. Therefore, it is meaningful to study the regeneration performance of catalyst for reuse. The regenerated catalyst was prepared by calcining the used catalyst from ambient temperature to 600 °C with a rate of 10 °C/min in an air atmosphere and maintained at 600 °C for 2 h. Compared with the fresh catalyst, the catalytic performance of regenerated catalyst was evaluated and shown in Fig. 10. It can be observed that the catalytic performance of regenerated catalyst for hydrogen-rich syngas production increased slightly. Among them, the H_2 content increased from 47.49% to 51.17%, and the CO content decreased from 13.15% to 12.72%. According to Fig. 3(a), the characteristic peak intensity of NiO in the regenerated catalyst was higher than that of the fresh Ni/Zr-MOF catalyst, which meant that NiO particles in the regenerated catalyst had better crystallinity. Therefore, the regenerated catalyst had better catalytic activity.

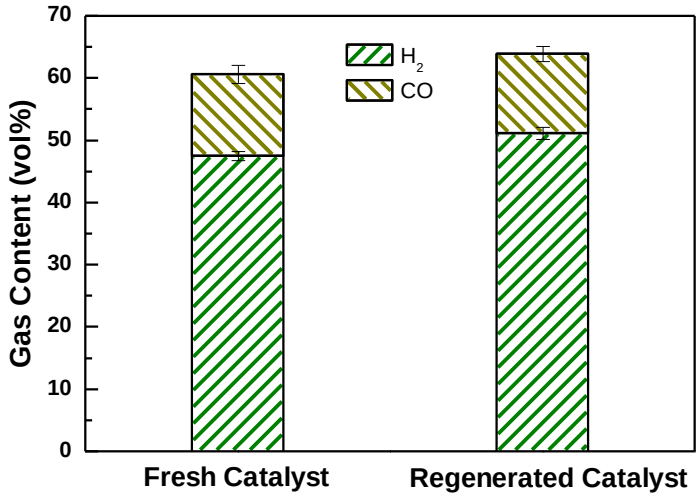

Fig. 10. Comparison of catalytic performance between fresh catalyst and regenerated catalyst

CONCLUSIONS

1. All of the Zr-MOF crystals took an octahedral shape with particle size of approximately 100 nm, and the Zr-MOF support had highly ordered mesoporous structure.
2. The Ni/Zr-MOF crystal was regular in shape, and most of them maintained the octahedral morphology. The metal nickel was uniformly dispersed on the surface of the Zr-MOF support.
3. After 10 tests, the sintering of catalyst resulted in the increase of nickel particle size from 10 to 12 nm. Due to the collapse of the catalyst structure and carbon deposition, the surface area and pore volume decreased from 132.7 to 5.64 m^2/g and 0.19 to 0.02 cm3/g, respectively.
4. The Ni/Zr-MOF catalyst showed high catalytic activity and thermal stability. With the Ni/Zr-MOF catalyst, the content of H_2 remarkably increased from 1.94 vol% to 47.49 vol%, and the H_2 yield increased from 0.39 mol/kg to 11.87 mol/kg.
5. The increase of Ni loading could promote the generation of hydrogen-rich syngas, but excessive nickel would agglomerate. 20 wt% was the optimal Ni loading for Ni/Zr-MOF catalyst.
6. After 10 tests, the Ni/Zr-MOF catalyst exhibited excellent cycle stability, and the H_2 content decreased from 48.22 vol% to 42.74 vol%. In addition, the H_2 yield decreased from 12.05 to 10.11 mol/kg, representing a decrease of only 16.1%.

ACKNOWLEDGMENTS

The authors are grateful for the support of the Technology Innovation Major Project of Hubei Province (No. 2017ABA155), the Central Committee Guide Local Science and Technology Development Special Project of Hubei Province (No. 2018ZYYD062), and the Hubei Provincial Natural Science Foundation of China (No. 2018CFB280).

REFERENCES CITED

Chan, F. L., and Tanksale, A. (2014). "Review of recent developments in Ni-based catalysts for biomass gasification," *Renew. Sust. Energ. Rev.* 38, 428-438. DOI: 10.1016/j.rser.2014.06.011

GB/T 212 (2008). "Proximate analysis of coal," Standardization Administration of China, Beijing, China.

Grams, J., Potrzebowska, N., Goscianska, J., Michalkiewicz, B., and Ruppert, A. M. (2016). "Mesoporous silicas as supports for Ni catalyst used in cellulose conversion to hydrogen rich gas," *Int. J. Hydrogen Energ.* 41(20), 8656-8667. DOI: 10.1016/j.ijhydene.2015.12.146

Guan, G., Kaewpanha, M., Hao, X., and Abudula, A. (2016). "Catalytic steam reforming of biomass tar: Prospects and challenges," *Renew. Sust. Energ. Rev.* 58, 450-461. DOI: 10.1016/j.rser.2015.12.316

Han, J., and Kim, H. (2008). "The reduction and control technology of tar during biomass gasification/pyrolysis: An overview," *Renew. Sust. Energ. Rev.* 12(2), 397-416. DOI: 10.1016/j.rser.2006.07.015

Hu, M., Guo, D., Ma, C., Hu, Z., Zhang, B., Xiao, B., Luo, S., and Wang, J. (2015). "Hydrogen-rich gas production by the gasification of wet MSW (municipal solid waste) coupled with carbon dioxide capture," *Energy* 90(Part 1), 857-863. DOI: 10.1016/j.energy.2015.07.122

Hu, M., Laghari, M., Cui, B., Xiao, B., Zhang, B., and Guo, D. (2018). "Catalytic cracking of biomass tar over char supported nickel catalyst," *Energy* 145, 228-237. DOI: 10.1016/j.energy.2017.12.096

Ismail, T. M., and El-Salam, M. A. (2017). "Parametric studies on biomass gasification process on updraft gasifier high temperature air gasification," *Appl. Therm. Eng.* 112, 1460-1473. DOI: 10.1016/j.applthermaleng.2016.10.026

Kunkes, E. L., Simonetti, D. A., West, R. M., Juan Carlos, S.-R., Gärtner, C. A., and Dumesic, J. A. (2008). "Catalytic conversion of biomass to monofunctional hydrocarbons and targeted liquid-fuel classes," *Science* 322(5900), 417-421. DOI: 10.1126/science.1159210

Quan, C., Gao, N. B., and Wu, C. F. (2017). "Utilization of NiO/porous ceramic monolithic catalyst for upgrading biomass fuel gas," *J. Energy Inst.* 91(3), 1-8. DOI: 10.1016/j.joei.2017.02.008

Ren, J., Langmi, H. W., North, B. C., Mathe, M., and Bessarabov, D. (2014). "Modulated synthesis of zirconium-metal organic framework (Zr-MOF) for hydrogen storage applications," *Int. J. Hydrogen Energ.* 39(2), 890-895. DOI: 10.1016/j.ijhydene.2013.10.087

Saxena, R. C., Adhikari, D. K., and Goyal, H. B. (2009). "Biomass-based energy fuel through biochemical routes: A review," *Renew. Sust. Energ. Rev.* 131, 167-178. DOI: 10.1016/j.rser.2007.07.011

Shen, W., Momoi, H., Komatsubara, K., Saito, T., Yoshida, A., and Naito, S. (2011). "Marked role of mesopores for the prevention of sintering and carbon deposition in dry reforming of methane over ordered mesoporous Ni-Mg-Al oxides," *Catal. Today* 171(1), 150-155. DOI: 10.1016/j.cattod.2011.04.003

Shen, Y., and Yoshikawa, K. (2013). "Recent progresses in catalytic tar elimination during biomass gasification or pyrolysis—A review," *Renew. Sust. Energ. Rev.* 21, 371-392. DOI: 10.1016/j.rser.2012.12.062

Shen, Y., Zhao, P., Shao, Q., Ma, D., Takahashi, F., and Yoshikawa, K. (2014). "*In-situ* catalytic conversion of tar using rice husk char-supported nickel-iron catalysts for biomass pyrolysis/gasification," *Appl. Catal. B-Environ.* 152-153, 140-151. DOI: 10.1016/j.apcatb.2014.01.032

Wu, C., Wang, L., Williams, P. T., Shi, J., and Huang, J. (2011). "Hydrogen production from biomass gasification with Ni/MCM-41 catalysts: Influence of Ni content," *Appl. Catal. B-Environ.* 108-109, 6-13. DOI: 10.1016/j.apcatb.2011.07.023

Xie, Y., Su, Y., Wang, P., Zhang, S., and Xiong, Y. (2018). "*In-situ* catalytic conversion of tar from biomass gasification over carbon nanofibers- supported Fe-Ni bimetallic catalysts," *Fuel Process. Technol.* 182, 77-87. DOI: 10.1016/j.fuproc.2018.10.019

Xu, X., Zhao, B., Sun, M., Chen, X., Zhang, M., Li, H., and Xu, S. (2017). "Co-pyrolysis characteristics of municipal sewage sludge and hazelnut shell by TG-DTG-MS and residue analysis," *Waste Manage.* 62, 91-100. DOI: 10.1016/j.wasman.2017.02.012

Yang, Y., Zhu, J., Zhu, G., Yang, L., and Zhu, Y. (2018). "The effect of high temperature on syngas production by immediate pyrolysis of wet sewage sludge with sawdust," *J. Therm. Anal. Calorim.* 132(3), 1783-1794. DOI: 10.1007/s10973-018-7143-9

Zhang, Z., Hu, X., Zhang, L., Yang, Y., Li, Q., Fan, H., Liu, Q., Wei, T., and Li, C.-Z. (2019). "Steam reforming of guaiacol over Ni/Al_2O_3 and Ni/SBA-15: Impacts of support on catalytic behaviors of nickel and properties of coke," *Fuel Process. Technol.* 191, 138-151. DOI: 10.1016/j.fuproc.2019.04.001

Zhang, Z., Liu, L., Shen, B., and Wu, C. (2018). "Preparation, modification and development of Ni-based catalysts for catalytic reforming of tar produced from biomass gasification," *Renew. Sust. Energ. Rev.* 94, 1086-1109. DOI: 10.1016/j.rser.2018.07.010

Zhao, M., Florin, N. H., and Harris, A. T. (2009). "The influence of supported Ni catalysts on the product gas distribution and H_2 yield during cellulose pyrolysis," *Appl. Catal. B-Environ.* 92(1-2), 185-193. DOI: 10.1016/j.apcatb.2009.07.011

Zhou, Y., Wang, W., Sun, J., Fu, L., Song, Z., Zhao, X., and Mao, Y. (2017). "Microwave-induced electrical discharge of metal strips for the degradation of biomass tar," *Energy* 126, 42-52. DOI: 10.1016/j.energy.2017.03.008

Article submitted: October 31, 2019; Peer review completed: December 31, 2020; Revised version received: January 11, 2020; Accepted: January 12, 2020; Published: January 24, 2020.
DOI: 10.15376/biores.15.1.1716-1731